Supplemental Online Material
(manuscript submitted to Physical Review Letters)
Two-step melting in two dimensions: First-order liquid-hexatic transition
Etienne P. Bernard, Werner Krauth
25 August 2011

In this supplemental online material, we first discuss the event-chain Monte Carlo algorithm[21] and its implementation, the constant NV ensemble and the visualization method (Section I). We then present additional material in support of the first-order nature of the liquid-hexatic transition (Section II), on positional and orientational order (Section III), and on the estimation of different types of finite-size effects (Section IV). Finally, Section V presents an elementary computer program, which allows us to directly "see" the exponential decay of positional correlations in the hexatic phase, and the power-law decay in the solid.
NB: Figures of the main article and of this supplemental online material are referred to as "Fig. k and "Fig. Sk", respectively. The references are those of the main article.

I. METHODS

Simulations are performed for N disks of radius σ in a square box of length L and volume $V = L^2$ with periodic boundary conditions. The position $\mathbf{r}_k = (x_k, y_k)$ corresponds to the center of disk k. The density (packing fraction) η is defined as the fraction of space occupied by disks: $\eta = N\pi\sigma^2/V$.

A. Algorithm

The "SEC" version of the event-chain algorithm [21] breaking detailed balance yet conserving global balance is used (see Fig. S1). Moves are either in the $+x$ or the $+y$ direction, and in one move, $\propto \sqrt{N}$ disks are displaced. Time is measured in displacements per disk. We obtain $\sim 3 \times 10^6$ disk displacements per second on a single processor, for all N. Simulations were run during one year on a cluster of workstations with 128 processors.

The event-chain algorithm is about two orders of magnitude faster than the local Monte Carlo algorithm. Extensive tests at system sizes where the local algorithm still thermalizes (see Fig. S2, and also [21] Fig. 3) show that the results of the event-chain algorithm agree

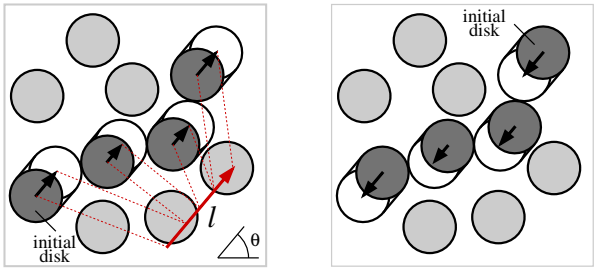

Figure S 1. Event-chain algorithm [21] for hard disks in a periodic box. For each move, a chain of disks is displaced by a fixed total distance l (the added lengths of the arrows). The algorithm is rejection-free. Detailed balance between the move and the return move is evident from the figure, but the algorithm can be sped up by moving only in the positive x direction or the positive y direction (it then breaks detailed balance but satisfies the weaker global balance condition).

with those of the local Monte Carlo algorithm. Although our algorithm is faster than previous methods, the correlation times are of the order of one week of CPU for the $N = 1,024^2$ system in the coexistence region. This corresponds to correlation times of the local Monte Carlo algorithm of more than one CPU year, not achieved in previous works with similar, or even larger systems [14, 15] (see Fig. 4).

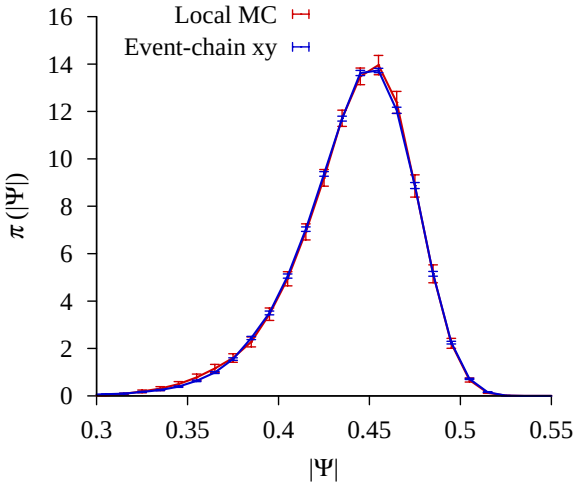

Figure S 2. Probability distribution for the absolute sample orientation. $|\Psi|$ is shown for $N = 256^2$ disks at density $\eta = 0.706$, for the event-chain algorithm used in this work and for the local Monte Carlo algorithm (see Fig. 3 of [21] for a related high-precision check using the integrated probability distribution of $|\Psi|$).

B. Statistics, error estimates

In an effort to save memory while achieving long run times, the protocol for the Monte Carlo computations was as follows (example for $N = 1,024^2$): Single event-chain simulations with 6×10^7 displacements per disk (about 9 months of computer time on a single processor) produced 64 essentially independent configurations which served as starting points of subsequent parallel simulations. The Gaussian error from these runs is indicated (see Fig. S3).

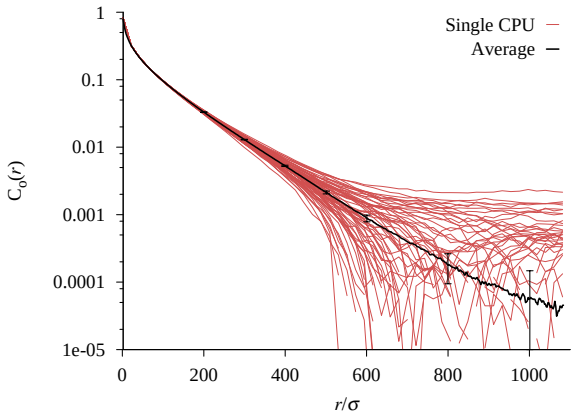

Figure S 3. Error computation for the orientational correlation functions. 64 independent initial configurations are obtained, equally spaced, from a 9-month Markov-chain calculation. In this example, the orientational correlation functions are evaluated in parallel. Gaussian error bars are shown.

C. Choice of ensemble, pressure

In order to study phase coexistence without the complication of an interface, it would be interesting to simulate at constant pressure, and especially in the so-called "Gibbs ensemble" consisting of two coupled simulation boxes. Both the constant-pressure ensemble and the Gibbs ensemble must implement volume changes in a system of N disks. Unfortunately, the volume autocorrelation time in Wood's classic constant-pressure algorithm (W. W. Wood, *J. Chem. Phys.* 48, 415 (1968), see also [19]) increases very strongly with N, and it becomes its limiting timescale. Modern versions of Wood's algorithm have not yet been able to solve this problem, and the development of efficient hard-sphere algorithms allowing for a change in volume (for large N) is an open problem.

In the constant-NV ensemble, the pressure is obtained from the contact value $g(2\sigma^+)$ of the two-particle correlation function

$$\beta P(2\sigma)^2 = \frac{4}{\pi}\eta[1 + 2\eta g(2\sigma^+)], \tag{1}$$

which is fitted at small distances through a high-order polynomial.

D. Orientational order parameter and its visualization

Disks (which are structureless) may be oriented with respect to their neighbors. The Voronoi construction yields neighborhood relations (see Fig. S4**a**) (two disks i and j are neighbors if the midpoint of the line connecting their centers is closer to i and j than to any other disk). The absolute value of Ψ_k, as defined in the main text, is equal to one if k and its neighbors are arranged as in a triangular lattice, and Ψ_k rotates by 2π if the lattice is rotated by an angle of $\pi/3$ without changing the reference axis. Ψ_k can be represented as a vector $(\mathrm{Re}\Psi_k, \mathrm{Im}\Psi_k)$ inside the disk k (see Fig. S4**b**). The color code considers the projection $\langle \Psi_k \hat{e}_\Psi \rangle$, where $\hat{e}_\Psi$ is the unit vector pointing in the direction of the sample orientation. The color code for Ψ_k can be applied to the vector inside the disk k (see Fig. S4**c**) and also to the Voronoi cell of k (see Fig. S4**d** and Fig. 1).

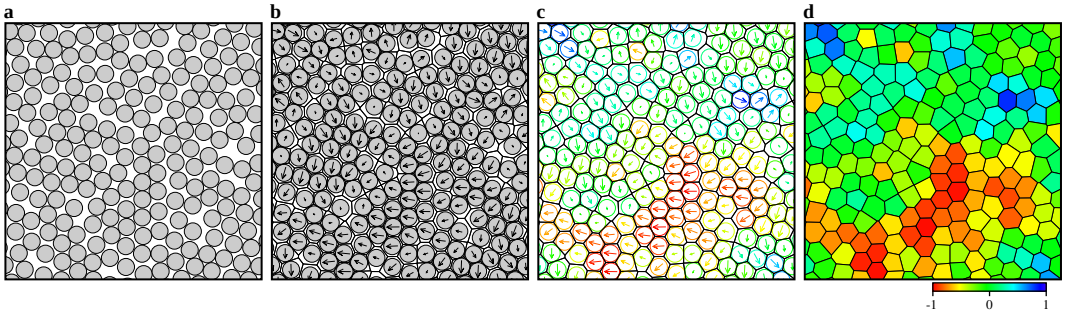

Figure S 4. Local orientational order and its visualization for a configuration of disks. Disks, shown in **a**, are oriented with respect to neighbors defined by the Voronoi construction (**b**). Color coding can be applied to the local orientations Ψ_k (**c** see also Fig. 1**b**,**c**,**d**), and to the entire Voronoi cell (**d**), as for example in Fig. 2 and Fig. 4.

II. CHARACTERIZATION OF THE FIRST-ORDER TRANSITION

To complement the data of Fig. 1, we show in Fig. S5 the synopsis of local orientations and coarse-grained densities for snapshots in the coexistence region. High density (~ 0.716) and local orientation along the sample orientation Ψ (blue regions) are clearly correlated.

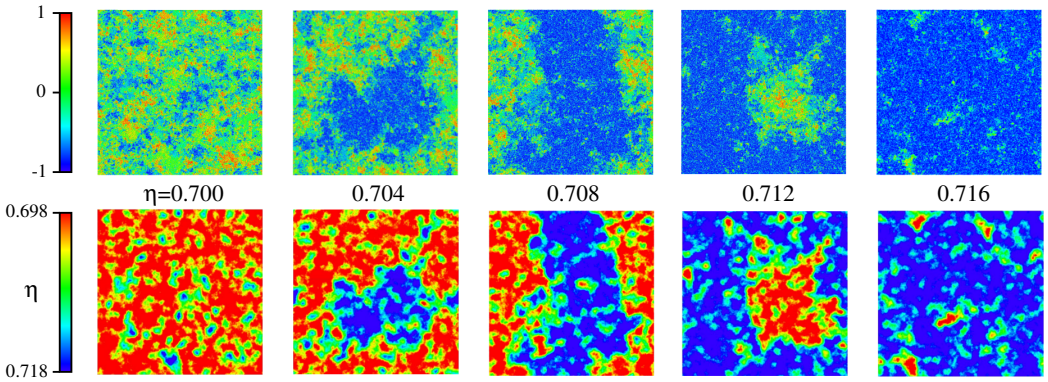

Figure S 5. Synopsis of orientation (upper) and coarse-grained density (lower) for snapshots in the coexistence region. The oriented regions (blue, upper panels) inside configurations are at density ~ 0.716 (red, lower panels), while liquid regions are at densities ~ 0.700. The upper panels in this figure are as in Fig. 2.

III. POSITIONAL AND ORIENTATIONAL ORDER, CORRELATION FUNCTIONS

In this section, we present additional results for the analysis of the crucial positional and orientational correlations. For the positional order, this involves an assessment of the correct positioning of the wave vector carrying the longest correlations.

A. Positional order, single configurations

All information on positional order is obtained from the two-dimensional pair correlation function $g(\Delta\mathbf{r})$ which for a given configuration is proportional to the histogram of $\Delta\mathbf{r}_{ij} = \mathbf{r}_i - \mathbf{r}_j$, taking into account periodic boundary conditions. We first treat the case of a single configuration, for an example with $N = 1,024$.

Instead of the $N^2 \sim 10^{12}$ pairs i and j, we consider $\sim 10^9$ randomly chosen pairs i, j. To produce Fig. 6, pairs are discarded unless they belong to a certain number of windows $(\Delta x, \Delta y)$ with

$$-10\sigma < \Delta y < 10\sigma$$
$$\tilde{x} - 10\sigma < \Delta x < \tilde{x} + 10\sigma. \tag{2}$$

In Fig. 6, we plot such histograms corresponding to $\tilde{x}/\sigma \in (0, 50, 100, 200)$ for $\eta = 0.718$ and to $\tilde{x}/\sigma \in (0, 100, 200, 400)$ for $\eta = 0.720$. The program listed in Section V of this supplemental online material was used. For $\eta = 0.718$, the pair correlations disappear on a scale of roughly one hundred σ whereas, for $\eta = 0.720$, the correlations remain strong throughout the system.

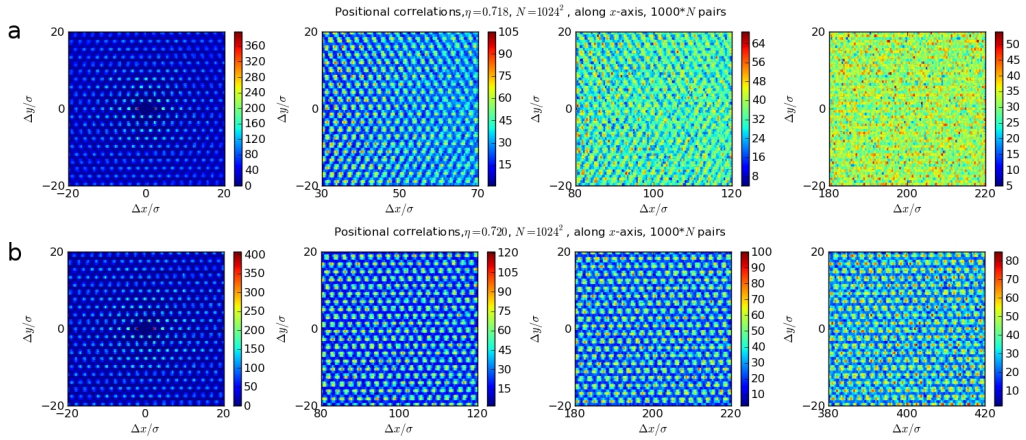

Figure S 6. Two-dimensional pair-correlation function for single configurations. The histogram for $g(\mathbf{r})$ is obtained by sampling 10^9 pairs i, j ($N = 1,024^2$). **a**: At density $\eta = 0.718$, positional order persists at distances of $\sim 100\sigma$, but it disappears at larger scales. **b**: Analogous histograms at density $\eta = 0.720$ show order throughout the system at much longer length scales (compare with Fig. 3). The two disk configurations, and the elementary computer program used to generate pair correlations from them, are made available (see Section V of this online material).

B. Positional order, average over configurations

For the quantitative analysis of positional correlations, presented in Fig. 3, each disk configuration is oriented with respect to the sample orientation Ψ. Using symmetry considerations, the two-dimensional histogram with about 10^7 slots and a resolution of $\sigma/5$ is

generated in 1/12 of the $\Delta x - \Delta y$ plane. The excellent signal-to-noise ratio in Fig. 3**b** is due to the use of a total of $\sim 10^{12}$ pair distances.

C. Positional order, correlation functions

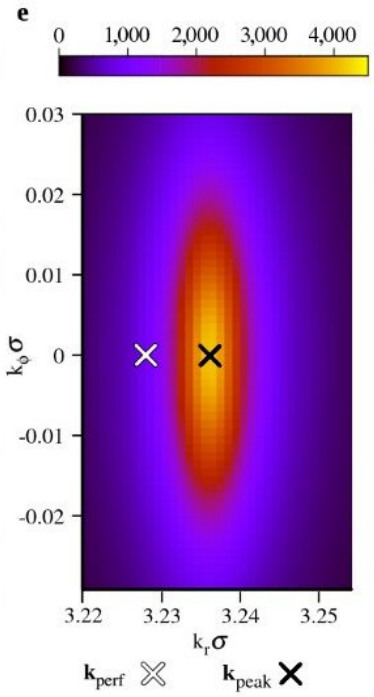

Figure S 7. Configuration-averaged structure factor $S(\mathbf{k})$ (one of the six first Bragg peaks) at $\eta = 0.718$. In this work, positional correlation functions $c_{\mathbf{k}}(r)$ are taken at the peak value $\mathbf{k}_{\text{peak}}$ of S, which is determined numerically. The reciprocal vector of the perfect triangular lattice at density η, $\mathbf{k}_{\text{perf}}$, (white cross) neglects the change of the lattice spacing by defects.

The configuration-averaged pair-correlation is modulated by a wave-vector clearly visible in the inset of Fig. 3**b**. This wave vector is given by the peak value $\mathbf{k}_{\text{peak}}$ of the two-dimensional structure factor $S(\mathbf{k}) = 1+N/V \int d^2\mathbf{r}(g(\mathbf{r})-1)\exp(i\mathbf{kr})$. The vector $\mathbf{k}_{\text{peak}}$ differs strongly from the wave-vector $\mathbf{k}_{\text{perf}}$ of the perfect triangular lattice of density η, contradicting what was assumed earlier [15, 18] (see Fig. S7). We determine $\mathbf{k}_{\text{peak}}$ numerically from the first Bragg peaks, and then obtain the positional correlation function, with $\mathbf{r} = (r, \phi)$, as $c_{\mathbf{k}}(r) = \int d\phi g(r,\phi)\exp(i\mathbf{kr}) / \int d\phi g(r,\phi)$ (see Fig. S7). The decay of $c_{\mathbf{k}}(r)$ agrees with the picture of Fig. 3 (which supposes no prior knowledge of $\mathbf{k}$).

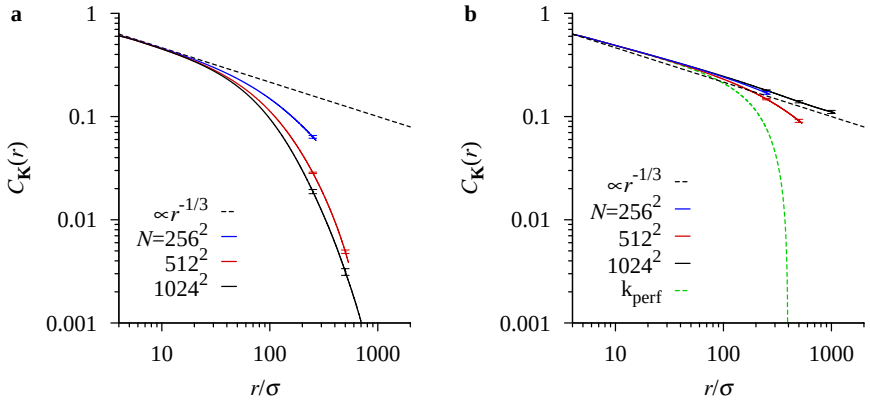

Figure S 8. Positional correlation functions. **a**: Positional correlation function at density $\eta = 0.718$, taken at the peak wave vector of the structure factor $s(\mathbf{k}_{\text{peak}})$, decay exponentially, in agreement with the two-dimensional pair correlation of Fig. 3**b**. At density $\eta = 0.720$ (**b**), $c_{\mathbf{k}}(r)$ decays approximately as $r^{-1/3}$ for the peak wave vector (in agreement with Fig. 3**b**), and unphysically fast for the wave vector $\mathbf{k}_{\text{perf}}$ of the perfect triangular lattice.

The spectacular increase of the positional correlation function for large r between $\eta = 0.718$ and $\eta = 0.720$, at the onset of solid order, can only be observed at $\mathbf{k}_{\text{peak}}$, as already evident from Fig. 3**b**. To illustrate this, we show in Fig. S8 the positional correlation function $c_{\mathbf{k}}(r)$ for the perfect-lattice value "k_{perf}". These correlations decay more quickly, with an unphysical inverse length scale given by $|\mathbf{k}_{\text{peak}} - \mathbf{k}_{\text{perf}}|$. To our knowledge, all previous works on two-dimensional melting used $\mathbf{k}_{\text{perf}}$ rather than $\mathbf{k}_{\text{peak}}$.

D. Orientational correlation functions

Orientational correlations can also be computed (see Fig. S9). At density $\eta = 0.700$, in the liquid phase, they decay exponentially, with a correlation length of $\sim 110\sigma$ much smaller than the system size. At density $\eta = 0.718$, in the hexatic phase, the orientational correlation function decays extremely slowly, but they cannot be long-range, because of the exponentially decaying positional order.

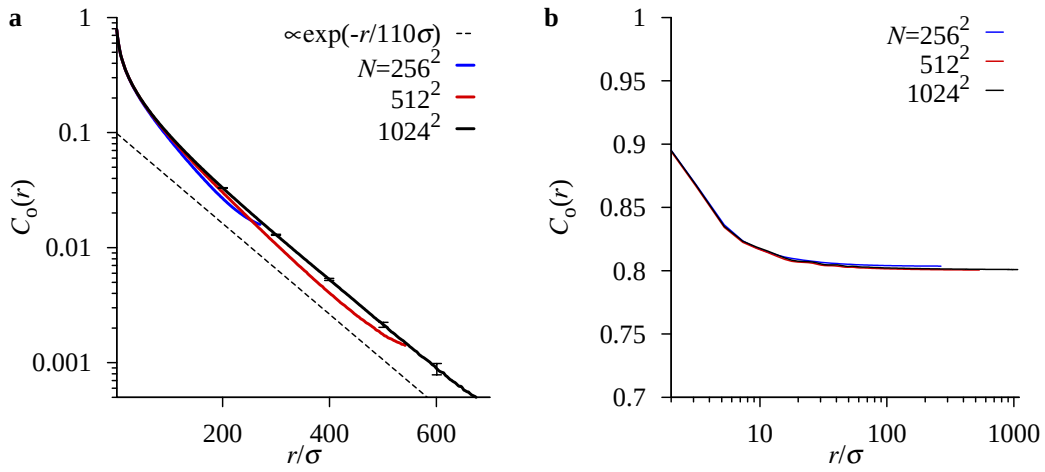

Figure S 9. Orientational correlation functions. At density $\eta = 0.700$ (**a**), $c_O(r)$ decays exponentially with a correlation length $\sim 110\sigma$. At density $\eta = 0.718$ (**b**), the decay is extremely slow, but correlations cannot be long-range because of the exponentially decaying positional order. This density is close to the transition into the solid phase, where the correlations decay with an exponent approaching zero.

IV. FINITE-SIZE EFFECTS

In this section, we study finite-size effects for correlation functions and density fluctuations.

A. Finite-size effects and positional and orientational order

As discussed in the main text, the systems of size up to $N = 1,024^2$ used in this study are large enough to exclude finite size effects (besides the effects due to the interface free energy in the coexistence window). The positional correlation length of the liquid in the coexistence region is very small, of the order of a few radii. The orientational correlation length of the coexisting liquid phase (identical to the orientational correlation at $\eta = 0.700$) is about $\sim 110\sigma$ (see Fig. S9). Smaller than the system size for $N = 512^2$ and $N = 1,024^2$, the correlation function changes very little with N.

In the coexistence window, the positional correlation length of the hexatic phase (see Fig. S8**a**) is smaller than the one at $\eta = 0.718$, thus smaller than $\sim 100\sigma$ (see Fig. S9**a**). Again, these correlations are smaller than the system size for $N = 512^2$ and $N = 1,024^2$,

and they vary little with N.

These considerations are confirmed by the collapse of $P(v)$ for $N = 512^2$ and $N = 1,024^2$ outside of the coexistence window.

B. Density fluctuations in the pure hexatic phase

The hexatic phase is quite narrow (between $\eta = 0.716$ and $\eta = 0.720$) but, in our largest systems, this density interval can easily be resolved. To show this, we determine the density fluctuations of a subsystem of size $N = 1,024^2$ in an infinite system: In the (T, P) ensemble, the volume fluctuations are related to the change of the pressure with volume:

$$\langle V^2 \rangle - \langle V \rangle^2 = -\partial \langle V \rangle / \partial (\beta P). \tag{3}$$

Using the derivative of the equation of state (see Fig. 2) at $\eta = 0.718$, it follows that the rms density fluctuations are $(\Delta\eta) = 2 \times 10^{-4}$, that is, one order of magnitude smaller than the distance to the phase boundaries. This result is confirmed by a direct observation of density fluctuations at different length scales.

In conclusion, for a system of $N = 1,024^2$ particles, in the range $\eta \in [0.716, 0.720]$, the NV and the NP ensemble are practically identical, and the density fluctuations in the NP ensemble are quite small.

V. COMPUTER PROGRAM FOR POSITIONAL CORRELATIONS

The following computer program (written in Python) generates Fig. 6, that is, the positional correlations for a single configuration of disks. The essential argument (the system at $\eta = 0.718$ has very long *orientational* but exponentially decaying *positional* correlations, it can therefore not be a solid) can thus be checked directly, without the more involved reasoning of Section III B, and with negligible programming effort (Bragg peaks and Voronoi cells need not be computed).

After reading in the configuration from file, $M \times N$ pair-distances are computed (out of the N^2 ones) and possibly binned in the histograms. Two sample configuration files (for $N = 1,024^2$ with $\eta = 0.718$ and $\eta = 0.720$) are available online.

```
##=======+=========+=========+=========+=========+=========+
```

```
## PROGRAM : correlation_position.py
## PURPOSE : positional correlations for a single config.
##           of N= 1024^2 disks in a square box of length 1.
## I/O     : Input configuration from file "config_0_718.dat",
##           histogram output into "correlation_0.718.png".
## LANGUAGE: Python 2.7
##========+=========+=========+=========+=========+=========+
import numpy, math, random
import  matplotlib.pyplot as plt
x=numpy.loadtxt('config_0_718.dat')
N=1048576
sigma =0.00046686  #  for eta=0.718
delta=20*sigma
x_dist=[0,50*sigma,100*sigma,200*sigma]
x_draw=[[],[],[],[]]
y_draw=[[],[],[],[]]
M=100   # run-time: 10 minutes. For fig S 7, M=1000 was used
for k in xrange(M*N):
   i = numpy.random.randint(0,N)
   j = numpy.random.randint(0,N)
   yy=(x[j,1]-x[i,1])%1.0
   if yy > 0.5: yy-=1.0
   if abs(yy) < delta:
      xx=(x[j,0]-x[i,0])%1.0
      if xx > 0.5: xx-=1.0
      for k in range(4):
         if abs(xx-x_dist[k]) < delta and i!=j:
            x_draw[k].append(xx/sigma)
            y_draw[k].append(yy/sigma)
plt.figure(figsize=(18,3.2))
plt.suptitle('Positional correlations')
plt.subplots_adjust(wspace=.3,bottom=0.15,top=0.85)
```

```
for k in range(4):
   plt.subplot(1,4,k+1)
   ymin=-20
   ymax=20
   xmin=x_dist[k]/sigma - 20
   xmax=x_dist[k]/sigma + 20
   plt.hexbin(x_draw[k],y_draw[k], gridsize=100)
   plt.axis([xmin,xmax,ymin,ymax])
   plt.xlabel("$\Delta x/\sigma$")
   plt.ylabel("$\Delta y/\sigma$",x=30.)
   plt.yticks([-20,0,20])
   plt.xticks([xmin,xmin+20,xmax])
   cb = plt.colorbar()
plt.savefig('correlation_0.718.png')
```